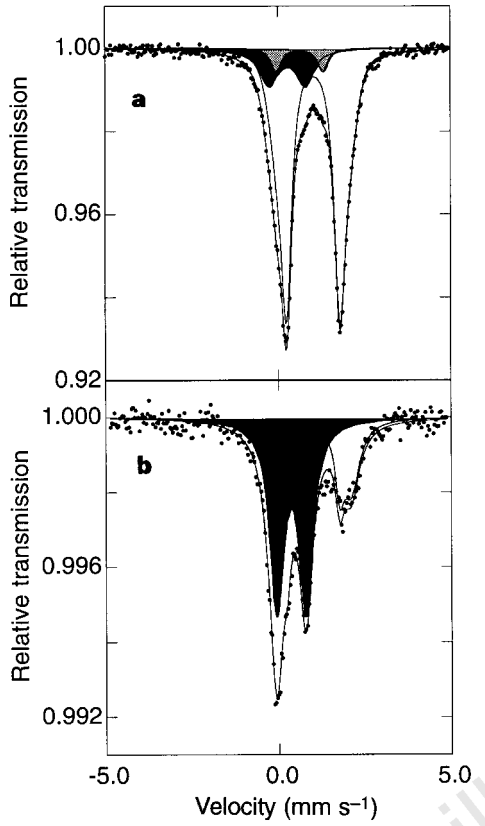

Figure 1 Mössbauer spectra of $(Mg,Fe)SiO_3$ perovskite: **a**, Al-free; **b**, containing 3.3 wt% Al_2O_3. Fe^{3+} absorption is shown as black in the spectra and peaks due to Fe^{2+}–Fe^{3+} electron transfer are shaded grey. Fe^{2+} absorption is modelled by two doublets which are thought to arise from differences in next-nearest neighbour environments[8]. Note the dramatic increase in relative Fe^{3+} content of the perovskite in the presence of Al.

above strongly suggests that it is significantly higher than currently believed.

Replacement of Fe^{2+} with Fe^{3+} in the perovskite phase is likely to affect significantly physical and chemical properties of the lower mantle such as sub- and super-solidus phase relations, transport properties, mechanical behaviour, trace-element partitioning and the concentration of species such as OH^-. For example, comparison of lower-mantle electrical conductivity models with laboratory measurements of lower-mantle phases in the system MgO–FeO–SiO_2 have been controversial (ref. 18 and references therein). Based on the present results, however, samples containing Al would be more representative of the lower mantle. Electrical-conductivity measurements of natural orthopyroxene show that addition of small amounts of Al_2O_3 increases electrical conductivity significantly, and that conductivity is relatively independent of oxygen fugacity[19]. By analogy with pyroxene, it is likely that electrical conductivity of $(Mg,Fe,Al)SiO_3$ perovskite would also be significantly higher than for the Al-free phase, as the conductivity mechanism is believed to involve Fe^{3+} (ref. 20). Laboratory measurements of electrical conductivity on Al-containing $(Mg,Fe)SiO_3$ perovskite are therefore required before a realistic comparison with bulk geophysical data can be made. □

Received 5 December 1996; accepted 22 April 1997.

1. Ito, E., Takahashi, E. & Matsui, Y. The mineralogy and chemistry of the lower mantle: an implication of the ultrahigh-pressure phase relations in the system MgO-FeO-SiO_2. *Earth Planet. Sci. Lett.* **67,** 238–248 (1984).
2. Guyot, F., Madon, M., Peyronneau, J. & Poirier, J. P. X-ray microanalysis of high-pressure/high-temperature phases synthesized from natural olivine in a diamond anvil cell. *Earth Planet. Sci. Lett.* **90,** 52–64 (1988).
3. Fei, Y., Mao, H. K. & Mysen, B. O. Experimental determination of element partitioning and calculation of phase relations in the MgO-FeO-SiO_2 system at high pressure and high temperature. *J. Geophys. Res.* **96,** 2157–2169 (1991).
4. Kesson, S. E. & Fitz Gerald, J. D. Partitioning of MgO, FeO, NiO, MnO and Cr_2O_3 between magnesian silicate perovskite and magnesiowüstite: Implications for the origin of inclusions in diamond and the composition of the lower mantle. *Earth Planet. Sci. Lett.* **111,** 229–240 (1991).
5. O'Neill, B. & Jeanloz, R. $MgSiO_3$-$FeSiO_3$-Al_2O_3 in the Earth's lower mantle: Perovskite and garnet at 1,200 km depth. *J. Geophys. Res.* **99,** 19901–19915 (1994).
6. Keppler, H., McCammon, C. A. & Rubie, D. C. Crystal field and charge transfer spectra of $(Mg,Fe)SiO_3$ perovskite. *Am. Mineral.* **79,** 1215–1218 (1994).
7. McCammon, C. A., Rubie, D. C., Ross, C. R., Seifert, F. & O'Neill, H. S. C. Mössbauer spectra of $^{57}Fe_{0.05}Mg_{0.95}SiO_3$ perovskite at 80 and 298 K. *Am. Mineral.* **77,** 894–897 (1992).
8. Fei, Y., Virgo, D., Mysen, B. O., Wang, Y. & Mao, H. K. Temperature dependent electron delocalization in $(Mg,Fe)SiO_3$ perovskite. *Am. Mineral.* **79,** 826–837 (1994).
9. McCammon, C. A. The crystal chemistry of ferric iron in $Fe_{0.05}Mg_{0.95}SiO_3$ as determined by Mössbauer spectroscopy. *Phys. Chem. Miner.* (submitted).
10. Pownceby, M. I. & O'Neill, H. S. C. Thermodynamic data from redox reactions at high temperatures. IV. Calibration of the Re-ReO_2 oxygen buffer from EMF and NiO + Ni\hbox -Pd redox sensor measurements. *Contrib. Mineral. Petrol.* **118,** 130–137 (1994).
11. McCammon, C. A. Crystal chemistry of iron-containing perovskites. *Phase Transitions* **58,** 1–26 (1996).
12. Kesson, S. E., Fitz Gerald, J. D., Shelley, J. M. G. & Withers, R. L. Phase relations, structure and crystal chemistry of some aluminous silicate perovskites. *Earth Planet. Science Lett.* **134,** 187–201 (1995).
13. Wood, B. J. & Rubie, D. C. The effect of alumina on phase transformations at the 660-kilometer discontinuity from Fe-Mg partitioning experiments. *Science* **273,** 1522–1524 (1996).
14. Farges, F., Guyot, F., Andrault, D. & Wang, Y. Local structure around Fe in $Mg_{0.9}Fe_{0.1}SiO_3$ perovskite: An X-ray absorption spectroscopy study at Fe-K edge. *Eur. J. Mineral.* **6,** 303–312 (1994).
15. Irifune, T. Absence of an aluminous phase in the upper part of the Earth's lower mantle. *Nature* **370,** 131–133 (1994).
16. McCammon, C. A., Harris, J. W., Harte, B. & Hutchison, M. T. Partitioning of ferric iron between lower mantle phases: Results from natural and synthetic samples. *J. Conf. Abstr.* **1,** 390 (1996).
17. Speidel, D. H. Phase equilibria in the system MgO-FeO-Fe_2O_3: The 1300 °C isothermal section and extrapolations to other temperatures. *J. Am. Ceram. Soc.* **50,** 243–248 (1967).
18. Duba, A. G. & Wanamaker, B. J. DAC measurement of perovskite conductivity and implications for the distribution of mineral phases in the lower mantle. *Geophys. Res. Lett.* **21,** 1643–1646 (1994).
19. Huebner, J. S., Duba, A. & Wiggins, L. B. Electrical conductivity of pyroxene which contains trivalent cations: Laboratory measurements and the lunar temperature profile. *J. Geophys. Res.* **84,** 4652–4656 (1979).
20. Poirier, J. P. & Peyronneau, J. in *High-Pressure Research: Application to Earth and Planetary Sciences* (eds Syono, Y. & Manghnani, M. H.) 77–87 (Terra Scientific/American Geophysical Union, Tokyo/Washington DC, 1992).

Acknowledgements. The manuscript was improved through discussions with A. Duba, B. Harte, M. Hutchison, S. Lauterbach, J. Peyronneau, J.-P. Poirer, F. Seifert and F. Visocekas. The sample of natural orthopyroxene was provided by J. Peyronneau and J.-P. Poirier, and the spectrum of the Al-perovskite phase was recorded at 80 K by S. Lauterbach. Mössbauer experiments were performed using equipment provided by F. Seifert, who was supported by Fonds der Chemischen Industrie (Germany).

Correspondence should be addressed to C.McC. (e-mail: catherine.mccammon@uni-bayreuth.de).

Luminescence dating of rock art and past environments using mud-wasp nests in northern Australia

Richard Roberts*, Grahame Walsh†, Andrew Murray‡, Jon Olley§, Rhys Jones‖, Michael Morwood¶, Claudio Tuniz#, Ewan Lawson#, Michael Macphail‖, Doreen Bowdery‖ & Ian Naumann☆

* *School of Earth Sciences, La Trobe University, Melbourne, Victoria 3083, Australia*
† *Takarakka Rock Art Research Centre, Carnarvon Gorge, Queensland 4702, Australia*
‡ *Nordic Laboratory for Luminescence Dating, Risø National Laboratory, DK 4000 Roskilde, Denmark*
§ *CSIRO Land and Water, Canberra, Australian Capital Territory 2601, Australia*
‖ *Division of Archaeology and Natural History, RSPAS, Australian National University, Canberra, Australian Capital Territory 0200, Australia*
¶ *Department of Archaeology and Palaeoanthropology, University of New England, Armidale, New South Wales 2351, Australia*
# *Physics Division, Australian Nuclear Science and Technology Organisation, Menai, New South Wales 2234, Australia*
☆ *CSIRO Entomology, Canberra, Australian Capital Territory 2601, Australia*

Mud-nesting wasps are found in all of the main biogeographical regions of the world[1–3], and construct nests that become petrified after abandonment. Nests built by mud-dauber and potter wasps in rock shelters in northern Australia[1,4] often overlie, and occasionally underlie, prehistoric rock paintings. Mud nests contain

pollen, spores and phytoliths from which information about local palaeovegetation can be gleaned. Here we report a new application of optical dating[5–7], using optically stimulated luminescence (OSL), and accelerator mass spectrometry (AMS) ^{14}C dating of pollen[8] to determine the ages of mud-wasp nests associated with rock paintings in the Kimberley region of Western Australia[9,10]. Optical dating of quartz sand (including the analysis of individual grains) embedded in the mud of fossilized nests shows that some anthropomorphic paintings are more than 17,000 years old. Reconstructions of past local environments are also possible from the range of pollen and phytolith types identified. This approach should have widespread application to studies of rock-art dating and late Quaternary environmental change on continents where mud-wasps once lived and other sources of palaeoecological information are absent.

Optical dating provides a measure of the time since minerals, such as quartz, were last exposed to sunlight[5–7]. Mud-nesting wasps gather surface sediments from the margins of streams and pools, further exposing any quartz grains to sunlight during collection and transport of the mud. Final exposure to the sun occurs during construction of the nest in a rock shelter. Quartz grains embedded in a nest are hidden from sunlight and will accumulate the effects of the nuclear radiation flux to which they are exposed. This radiation dose (the palaeodose) will increase with time and may be measured using optically stimulated luminescence (OSL). Mud nests constructed originally by two species of mud-dauber wasp, *Sceliphron laetum* (Smith) and *Sceliphron formosum* (Smith)[11], and the eumenine (potter) wasp (*Abispa* spp.)[1,4] were collected from the rain-protected ceilings and recesses of rock shelters in the northern Kimberley region of Australia. Nests were removed at night, using red-filtered (>590 nm) light, without damage to the paintings. Most of these nests were built over paintings, the relative ages of which could be estimated from a sequence of superposed motif styles[9,10]. Seven nests were chosen for initial dating. Three lightly cemented *S. laetum* nests (DR1, DR2 and DR6) had been built over parts of red-pigmented Wandjina (anthropomorphic) figures in one rock shelter. At another site, the residual stump of a heavily cemented, probably *S. laetum*, nest (KERC4) directly overlay the head-dress of a mulberry-coloured human figure (which, in turn, overlay a hand stencil), and this nest thickened laterally into a much larger but similarly indurated nest (KERC5). The human figure in the painting has an elongated torso, hanging arms (no decorations visible) and a narrow head from whose apex radiates a semi-circular tufted head-dress; the painting looks archaic, and may be related to the Bradshaw style[9,10]. Two *S. laetum* nests, not obviously associated with any paintings, were also collected: an especially petrified nest (DR4) in the Wandjina rock shelter, and a 'modern' nest (KERC9, <2 years old). Nest KERC4 was no more than 5 mm thick, whereas the other nests were 20–40 mm thick.

To examine the opacity of a mud nest, the largest nest collected (DR6) was divided into seven portions, the first portion being composed of the outermost 1–3 mm of the nest mud, with successive portions consisting of mud concealed deeper within the nest; the 'core' portion had been attached to the shelter wall. Each portion was optically dated, the aim being to check that the inner portions of the nest were sufficiently light-safe to retain an OSL signal. Nest DR4 was divided into an inner core and an outer shell, while only the cores of nests DR1, DR2, KERC9 and KERC5 were dated. Quartz grains were extracted from each portion, and palaeodoses were determined using the standard multiple-aliquot additive-dose procedure[12], or the newly devised single-aliquot additive-dose and regenerative-dose protocols[13–15]. Nest KERC4 required a different approach because of its small size: quartz grains were extracted from the entire nest and, as there were insufficient grains for standard multi-grain analysis, individual grains were dated using single-aliquot protocols. A frequency

Table 1 Dose rates, palaeodoses and optical dates for quartz grains, and AMS ^{14}C determinations for pollen grains

		Dose rate* (mGy y^{-1})				Palaeodose (Gy)‡			OSL age (y)§	AMS ^{14}C determinations		
Mud nest	Portion of nest	γ- and cosmic ray (1)†	γ- and cosmic ray (2)†	Nest mud β	Total dose rate					Sample code	Pollen diameter (μm)	^{14}C activity (% M)‖
KERC9	Core	0.41 ± 0.02	no data	0.56 ± 0.02	0.99 ± 0.03	0.15 ± 0.02	SA	(24)	150 ± 20	OZC361	<5	85.0 ± 1.0
										OZC362	5–10	111.1 ± 2.1
										OZC363	10–25	111.2 ± 1.1
										OZC364	45–90	111.4 ± 1.2
DR1	Core	0.61 ± 0.03	0.66 ± 0.03	0.63 ± 0.03	1.29 ± 0.04	0.13 ± 0.01	SA	(24)	100 ± 10			
DR2	Core	0.49 ± 0.03	0.52 ± 0.03	0.97 ± 0.04	1.51 ± 0.04	0.22 ± 0.01	SA	(21)	150 ± 10	OZC357	<5	88.4 ± 0.7
										OZC358	5–10	98.9 ± 3.1
										OZC359	10–25	92.4 ± 1.1
										OZC360	45–90	101.0 ± 2.7
DR6	Layer 1	0.50 ± 0.03	0.50 ± 0.03	0.87 ± 0.04	1.32 ± 0.04	0.14 ± 0.02	M	(20)	110 ± 20			
	Layer 2	0.50 ± 0.03	0.50 ± 0.03	0.87 ± 0.04	1.40 ± 0.04	0.35 ± 0.06	M	(19)	250 ± 50			
	Layer 3	0.50 ± 0.03	0.50 ± 0.03	0.87 ± 0.04	1.40 ± 0.04	0.36 ± 0.04	M	(18)	260 ± 30			
						0.41 ± 0.03	SA	(15)	290 ± 30			
	Layer 4	0.50 ± 0.03	0.50 ± 0.03	0.87 ± 0.04	1.40 ± 0.04	0.35 ± 0.04	M	(20)	250 ± 30			
	Layer 5	0.50 ± 0.03	0.50 ± 0.03	0.87 ± 0.04	1.40 ± 0.04	0.43 ± 0.08	M	(20)	310 ± 60			
	Layer 6	0.50 ± 0.03	0.50 ± 0.03	0.87 ± 0.04	1.40 ± 0.04	0.83 ± 0.12	M	(19)	590 ± 90			
	Layer 7	0.50 ± 0.03	0.50 ± 0.03	0.87 ± 0.04	1.40 ± 0.04	0.84 ± 0.17	M	(19)	600 ± 130			
						0.86 ± 0.06	SA	(3)	610 ± 50			
DR4	Outer shell	0.53 ± 0.03	no data	1.47 ± 0.07	2.05 ± 0.06	2.5 ± 0.2	M	(20)	1,240 ± 120			
	core	0.53 ± 0.03	no data	1.47 ± 0.07	2.05 ± 0.06	3.7 ± 0.4	M	(20)	1,810 ± 210			
						3.1 ± 0.4	SA	(6)	1,530 ± 220			
KERC5	Core	0.47 ± 0.02	0.50 ± 0.03	1.64 ± 0.08	1.89 ± 0.07	33 ± 3	SA	(6)	17,500 ± 1,800			
KERC4	Whole nest	0.47 ± 0.02	0.50 ± 0.03	1.64 ± 0.08	1.89 ± 0.07	45 ± 4	SA	(21)	23,800 ± 2,400			
						31 ± 3	SR	(15)	16,400 ± 1,800			

* Activities of ^{238}U and ^{232}Th decay series nuclides, and ^{40}K, are converted to dose rates (mean ± total uncertainty) using published relations[24,25].

† Estimate (1) is the sum of the *in situ* γ-ray dose rate (determined using a field γ-spectrometer, and high-resolution γ-spectrometry on powdered rock samples[26]), and the cosmic-ray dose rate estimated from published equations[27]. Estimate (2) is obtained from thermoluminescence dosimetry capsules (CaF_2 in copper) attached to the rock face for one year after nest collection (and corrected for travel dose, self-dose, and capsule-wall attenuation[12]).

‡ Mean palaeodose ± standard error, obtained by multiple-aliquot additive-dose (M), single-aliquot additive-dose (SA), and single-aliquot regenerative-dose (SR) protocols. Values in parentheses are the number of aliquots used for each multiple-aliquot determination of palaeodose, or the number of single-aliquot or single-grain (for KERC4) estimates of palaeodose.

§ Mean ± total uncertainty, calculated as the quadratic sum of the random and systematic uncertainties[12].

‖ Activity as percentage modern carbon, measured using the tandem accelerator mass spectrometer at ANSTO (ref. 28). A δ^{13}C value of −25‰ is assumed. Ages for samples OZC362, 363, 364, 358 and 360 are indistinguishable from modern, whereas uncalibrated ^{14}C ages for OZC361, 357 and 359 are 1,310 ± 100, 990 ± 60 and 640 ± 95 years BP, respectively. We have not yet determined the cause(s) of the three non-modern ages, although finely comminuted contaminants[29,30] are presumably involved.

distribution of single-grain palaeodoses is thereby obtained[15,16], enabling unilluminated grains to be discriminated from grains exposed to light near the surface.

The 'age profile' obtained for nest DR6 (Fig. 1, Table 1) indicates that only the outermost portion of the nest contains grains that have been exposed to modern sunlight, yielding an apparent age of 110 ± 20 years, with the next four portions having a weighted mean age of 270 ± 20 years. The two innermost portions have an average age of 610 ± 40 years, implying that DR6 consists of two generations of nest. This finding is consistent with the observation[1,17] that mud-dauber wasps prefer to build nests near existing nests and on the stumps of abandoned nests, rather than on a bare rock surface. The non-zero age of the outermost portion corresponds to a residual palaeodose of 0.14 ± 0.02 Gy, and similar palaeodoses were obtained from the cores of the recent nest KERC9 and nest DR1. The ages of 100–150 years for KERC9, DR1 and DR2 indicate the lower age limit that can be expected using OSL. Two further lines of evidence support a recent origin for these nests: first, the presence of 160–270% ^{210}Pb excess (presumably from atmospheric fallout) in nests DR1 and KERC9 indicates that these nests are built from mud collected within the last 100 years; and second, AMS ^{14}C determinations made on pollen grains[8] (>5 μm in diameter) extracted from nests DR2 and KERC9 give ages that are indistinguishable from modern (Table 1), indicating that the pollen is derived from plants flowering around the time of nest construction.

The core of nest DR4 yielded an optical date of ~1,800 years which, although it is not obviously associated with any painting, demonstrates the preservation potential of large nests. This is further borne out by the remarkable antiquity of nests KERC4 and KERC5. The core of the latter yielded an age of ~17,500 years, and the single grains dated from nest KERC4 suggest an age of more than 16,400 years for the underlying anthropomorphic painting. These results show that the mulberry-coloured human figure was painted at or before the Last Glacial Maximum, and that the underlying hand stencil must be older still. Independent support for a Pleistocene age is implied by the condition of equilibrium existing between ^{230}Th and ^{226}Ra in the mud from nest KERC5. Nests constructed in the past 600 years (DR1, DR2, DR6 and KERC9) exhibit disequilibrium between ^{230}Th and ^{226}Ra, owing to a 40–110% ^{226}Ra excess associated with the sediments used to build the nests. If KERC5 and KERC4 had been constructed of mud with a similar initial ^{226}Ra excess, it would have taken at least 8,000 years (five half-lives of ^{226}Ra) for this excess to decay away.

Nests of *S. laetum* (including DR1, DR2, KERC5 and KERC9), *S. formosum* and eumenine wasps have been examined for pollen, spores and phytoliths. Pollen is present in nest mud chiefly as a result of wasps visiting flowering plants for nectar. Phytoliths provide a record of polymerized biogenic silica which has been deposited in the source mud after release from plant organic material. Initial investigation of a *S. laetum* nest and eumenine wasp nest (both undated but probably late Holocene in age) showed that both were rich in pollen, yielding 1–2 mg of pollen from 1 g of mud. A large, distinctive pollen type produced by *Grevillea* or *Hakea* was predominant in the *S. laetum* nest, whereas a more equal representation of pollen types (eucalypt, ti-tree, paperbark, wattle, *Grevillea* and *Hakea*) was present in the eumenine wasp nest (Table 2). A diverse mix of abundant pollen was found subsequently in nests DR1, DR2 and KERC9, but an indurated *S. formosum* nest seemed to contain no pollen. Pleistocene nest KERC5 showed the presence of some Myrtaceae pollen, but not enough to allow AMS ^{14}C dating. These differences almost certainly reflect the particular foraging strategies of mud-dauber and potter wasps and perhaps some degradation of pollen with time. The types of phytolith extracted[18] from the mud of four dated *S. laetum* nests (Table 3) include varieties of grass and dicotyledon, as well as carbon particles, starch grains and, at the Wandjina site, freshwater sponge spicules. These samples did not contain a sufficient mass of phytolith for AMS ^{14}C dating, but other nests may prove amenable. Previous studies have used occluded carbon in phytoliths for AMS ^{14}C dating and palaeoclimatic reconstructions[19]. Further investigations of fossil pollen and phytolith types should allow a

Table 2 Pollen and spore types extracted from selected mud-wasp nests

Taxon	Main pollinator	Total pollen and spore count (%) Eumenine wasp nest*	*Sceliphron laetum* nest*	Nest KERC5
Eucalyptus type	insect	24	2	28
Leptospermum type	insect	15	1	–
Melaleuca type	insect	10	<1	–
Other Myrtaceae	insect	5	<1	51
Acacia	insect	38	1	2†
Grevillea/Hakea	insect	4	91	2†
Apiaceae	insect	1	<1	–
Chenopodiaceae	wind	–	<1	–
Asteraceae	insect	<1	<1	–
Haloragaceae	insect	<1	1	–
Poaceae	wind	–	2	2
Other angiosperms	insect	3	1	15†
Ferns	water	<1	<1	–
n§		2,357	1,875	47

Types not recorded are indicated by a dash.
* Nests are probably late Holocene in age.
† Modern contaminants, mostly in the 25–45 μm fraction.
§ *n*, Number of pollen grains and spores counted.

Table 3 Phytolith types extracted from selected *S. laetum* nests

Phytolith type	Nest DR1	Nest DR2	Nest KERC9	Nest KERC5
Grasses*				
B	–	Y	Y	Y
A	–	–	–	Y
AT	–	–	Y	–
OR	–	Y	Y	–
Dicotyledons†				
R	Y	Y	Y	Y
O	Y	–	Y	Y
Carbon particles	Y	Y	Y	–
Starch grains‡	20	20	20	16
Sponge spicules	Y	Y	–	–

Types recorded are indicated Y; types not recorded are indicated by a dash.
* Grass shapes: B, bilobe; A, angular; AT, arc/triangle; OR, ornamented rectangles.
† Dicotyledon and non-Poaceae monocotyledon shapes: R, rectangular; O, others.
‡ Approximate grain diameter (μm).

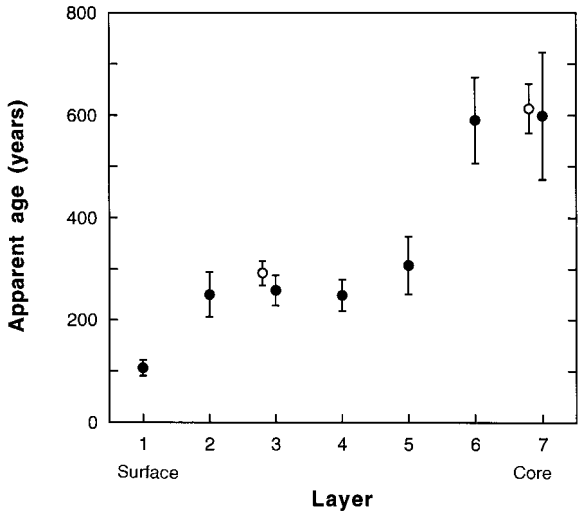

Figure 1 Optical dates obtained from each portion of *S. laetum* nest DR6 (40 mm from core to surface). Filled circles, mean ages (±1σ uncertainties) derived using a multiple-aliquot additive-dose protocol; open circles, mean ages derived using a single-aliquot additive-dose protocol. Note the concordance between multiple-aliquot and single-aliquot age estimates for layers 3 and 7.

detailed reconstruction of the palaeoenvironment for each interval of time represented by a nest.

The worldwide distribution of mud-wasps and the demonstrated longevity of their nests should prove a valuable tool in archaeological and palaeoclimatic research. The rapid formation and short period of usage of a nest, and the incorporation of a variety of palaeoecological indicators, makes each mud-wasp nest a 'snapshot' of its late Quaternary environment. By examining nests of different ages in several localities, it should be feasible to infer sequences of prehistoric human activity and vegetation change at various geographic scales and in climatic zones where other palaeoecological records are poorly preserved. Optical dating of single grains of sand now makes it possible to date very small nests, such as those produced by *S. formosum* (which typically overlie the stylistically oldest paintings), and the painted stumps of nests (to obtain maximum ages for art motifs). Sediment accretions created by some other animals (such as ants, termites and mud-nesting birds) may also be suitable for optical dating if the mineral grains were fully exposed to sunlight during final emplacement. □

Methods

Palaeodose determinations. Quartz grains 90–125 μm in diameter were extracted from the mud nests and then etched in 40% hydrofluoric acid for 45 min to remove the α-particle-dosed outer rinds. Multiple-aliquot additive-dose palaeodoses were obtained using conventional quartz dating procedures[6,20,21], a 300-s preheat at 220 °C, optical stimulation (500 ± 40 nm) at room temperature, and OSL emissions detected through 2.5-mm U-340 and 3-mm UG-11 filters. Single-aliquot additive-dose palaeodoses were obtained from successive short-shine/dose/preheat cycles, using a 10-s preheat at 160–300 °C (the preheat plateau[6] region was determined for each multi-grain sample and invariably included 280 °C), optical stimulation of 420–550 nm at 125 °C, and OSL emissions detected through two 3-mm U-340 filters[14,15,21]. A 10-s preheat at 280 °C was used for all single-grain analyses. Single-aliquot regenerative-dose palaeodoses were obtained using the same equipment, the total OSL signal from successive long-shine/dose/preheat cycles, and the 110 °C thermoluminescence signal to correct for differences in OSL sensitivity between cycles[15]. Laboratory $^{90}Sr/^{90}Y$ sources delivered β-particle doses at 22–48 mGy s^{-1}. OSL ages for nest KERC4 are calculated from individual grains with palaeodoses >10 Gy. The additive-dose and regenerative-dose palaeodoses (from 21 and 15 grains, respectively) show a broad, approximately gaussian, frequency distribution, which we interpret as reflecting grain-to-grain differences in dose-response behaviour and β-particle microdosimetry[15]. Grains with palaeodoses >10 Gy (33 grains with palaeodoses of 14–59 Gy and three grains with additive-dose palaeodoses of ~75 Gy) are presumed to be light-safe, whereas those with a smaller palaeodose (25% of the grains examined) are considered to have been exposed to modern sunlight, either on the surface of the nest or in the immediate subsurface where attenuated sunlight may penetrate sufficiently to partly empty the OSL traps. This problem does not apply to nest KERC5, from which grains were extracted only from the unilluminated core.

Dose rate determinations. The γ-ray dose is derived mostly from the local bedrock, with a minor (5%) γ-ray contribution from the nest mud. The cosmic-ray plus bedrock γ-ray dose rate was estimated by two independent methods for most nests (Table 1 footnote), and averaged to calculate nest ages. The β-particle dose rate is derived entirely from the nest mud and was calculated using an attenuation factor[22] of 0.93 ± 0.03. The only exceptions are layer 1 of DR6 (grains in this thin exterior layer are assumed to have received only 90% of the 4π β-particle dose rate), and nests KERC5 and KERC4 (for which a 25% contribution from bedrock (β-particle dose rate, 0.49 ± 0.03 mGy yr^{-1}) is assumed, owing to the close contact between the sampled grains and the rock surface, giving a total β-particle dose rate 18% smaller than if the β-particle flux were derived from the mud only). The β-particle dose rates from nest mud were deduced from X-ray fluorescence and α-particle spectrometry[23]. The latter analyses show that the ^{238}U decay series is in disequilibrium, with unsupported excesses of ^{210}Pb (in DR1 and KERC9) and ^{226}Ra (in DR1, DR2, DR6 and KERC9). A ^{210}Pb excess does not significantly affect the dose rate, and had KERC5 or KERC4 been formed with an initial ^{226}Ra excess of 100% then the dose rate (integrated over 20,000 years) would be <1% greater than the modern (equilibrium) dose rate used to calculate their OSL ages. The $^{210}Pb/^{226}Ra$ ratio for DR6 indicates ^{222}Rn emanation of 18%, which is assumed to have prevailed since nest construction. Because of the paucity of mud available for KERC4, the nest-derived β-particle dose rate is assumed to be the same as that determined for its lateral extension, KERC5. An internal α-particle and absorbed β-particle dose rate[22] of 0.02 ± 0.01 mGy yr^{-1} was deduced from U and Th concentrations in single grains of acid-etched quartz (measured by laser-ablation inductively coupled plasma mass spectrometry (ICP-MS) using a pulsed ArF excimer laser operating at 193 nm) and an assumed α-particle efficiency '*a*' value of 0.1. The dose rates require no moisture corrections as the nests are dry.

Received 4 February; accepted 17 April 1997.

1. Naumann, I. D. in *The Rock Art Sites of Kakadu National Park – Some Preliminary Research Findings for their Conservation and Management* (ed. Gillespie, D.) 127–189 (Special Publication 10, Australian National Parks and Wildlife Service, Canberra, 1983).
2. Gauld, I. D. & Bolton, B. (ed.) *The Hymenoptera* (Oxford Univ. Press, 1988).
3. LaSalle, J. & Gauld, I. D. (ed.) *Hymenoptera and Biodiversity* (C.A.B. International, Wallingford, 1993).
4. Naumann, I. D. in *The Insects of Australia: A Textbook for Students and Research Workers* 2nd edn, 916–1,000 (Melbourne Univ. Press, 1991).
5. Huntley, D. J., Godfrey-Smith, D. I. & Thewalt, M. L. W. Optical dating of sediments. *Nature* **313,** 105–107 (1985).
6. Aitken, M. J. Optical dating: a non-specialist review. *Quat. Sci. Rev.* **13,** 503–508 (1994).
7. Duller, G. A. T. Recent developments in luminescence dating of Quaternary sediments. *Prog. Phys. Geogr.* **20,** 127–145 (1996).
8. Brown, T. A., Nelson, D. E., Mathewes, R. W., Vogel, J. S. & Southon, J. R. Radiocarbon dating of pollen by accelerator mass spectrometry. *Quat. Res.* **32,** 205–212 (1989).
9. Walsh, G. L. *Bradshaws: Ancient Rock Paintings of North-West Australia* (The Bradshaw Foundation, Geneva, 1994).
10. Morwood, M. J., Walsh, G. L. & Watchman, A. The dating potential of rock art in the Kimberley, N.W. Australia. *Rock Art Res.* **11,** 79–87 (1994).
11. Smith, F. in *Catalogue of Hymenopterous Insects in the Collection of the British Museum* Part IV 207–497 (British Museum, London, 1856).
12. Aitken, M. J. *Thermoluminescence Dating* (Academic, London, 1985).
13. Duller, G. A. T. Luminescence dating using single aliquots: methods and applications. *Radiat. Meas.* **24,** 217–226 (1995).
14. Murray, A. S., Roberts, R. G. & Wintle, A. G. Equivalent dose measurement using a single aliquot of quartz. *Radiat. Meas.* **27,** 171–184 (1997).
15. Murray, A. S. & Roberts, R. G. Determining the burial time of single grains of quartz using optically stimulated luminescence. *Earth Planet. Sci. Lett.* (submitted).
16. Lamothe, M., Balescu, S. & Auclair, M. Natural IRSL intensities and apparent luminescence ages of single feldspar grains extracted from partially bleached sediments. *Radiat. Meas.* **23,** 555–561 (1994).
17. Waterhouse, D. F. in *The Insects of Australia: A Textbook for Students and Research Workers* 2nd edn, 221–235 (Melbourne Univ. Press, 1991).
18. Bowdery, D. E. thesis, Australian National Univ. (1996).
19. Kelly, E. F., Amundson, R. G., Marino, B. D. & Deniro, M. J. Stable isotope ratios of carbon in phytoliths as a quantitative method of monitoring vegetation and climate change. *Quat. Res.* **35,** 222–233 (1991).
20. Roberts, R. G. *et al.* The human colonisation of Australia: optical dates of 53,000 and 60,000 years bracket human arrival at Deaf Adder Gorge, Northern Territory. *Quat. Sci. Rev.* **13,** 575–583 (1994).
21. David, B., Roberts, R., Tuniz, C., Jones, R. & Head, J. New optical and radiocarbon dates from Ngarrabullgan Cave, a Pleistocene archaeological site in Australia: implications for the comparability of time clocks and for the human colonization of Australia. *Antiquity* **71,** 183–188 (1997).
22. Mejdahl, V. Thermoluminescence dating: beta-dose attenuation in quartz grains. *Archaeometry* **21,** 61–72 (1979).
23. Martin, P. & Hancock, G. Routine analysis of naturally occurring radionuclides in environmental samples by alpha-particle spectrometry. Supervising Scientist for the Alligator Rivers Region, Research Report 7 (Australian Government Publishing Service, Canberra, 1992).
24. Nambi, K. S. V. & Aitken, M. J. Annual dose conversion factors for TL and ESR dating. *Archaeometry* **28,** 202–205 (1986).
25. Olley, J. M., Murray, A. & Roberts, R. G. The effects of disequilibria in the uranium and thorium decay chains on burial dose rates in fluvial sediments. *Quat. Sci. Rev.* **15,** 751–760 (1996).
26. Murray, A. S., Marten, R., Johnston, A. & Martin, P. Analysis for naturally occurring radionuclides at environmental concentrations by gamma spectrometry. *J. Radioanal. Nuclear Chem. Articles* **115,** 263–288 (1987).
27. Prescott, J. R. & Hutton, J. T. Cosmic ray contributions to dose rates for luminescence and ESR dating: large depths and long-term time variations. *Radiat. Meas.* **23,** 497–500 (1994).
28. Tuniz, C. *et al.* The ANTARES AMS Centre: a status report. *Radiocarbon* **37,** 663–673 (1995).
29. Brown, T. A., Farwell, G. W., Grootes, P. M. & Schmidt, F. H. Radiocarbon AMS dating of pollen extracted from peat samples. *Radiocarbon* **34,** 550–556 (1992).
30. Long, A., Davis, O. K. & De Lanois, J. Separation and ^{14}C dating of pure pollen from lake sediments: nanofossil AMS dating. *Radiocarbon* **34,** 557–560 (1992).

Acknowledgements. We thank the traditional Aboriginal custodians (M. Pandilow, T. H. Unghango and family members, L. Utemara and D. Utemara, L. Karedada, J. Karedada and S. Mangolamara), Kalumburu Community Council and A. Koeyers for permission to undertake this study. Samples were collected under permits 166 and NE001023 from the Western Australian Aboriginal Affairs Department and Department of Conservation and Land Management, respectively. We thank D. Questiaux for preparing and E. Haskell for analysing the thermoluminescence dosimetry capsules; M. Shelley for preparing and L. Kinsley for measuring the laser-ablation ICP-MS samples; K. Weiss and G. Atkin for pollen extraction; G. Jacobsen for ^{14}C sample preparation; M. J. Olley for X-ray fluorescence analyses; and A. Bell and M. Aitken for comments. R.R. acknowledges the support of a Queen Elizabeth II fellowship from the Australian Research Council and a J. G. Russell Award from the Australian Academy of Science, which funded some of the research costs. The Bradshaw Foundation, Australian National University and Australian Research Council funded the fieldwork, and the Australian Institute of Nuclear Science and Engineering funded the AMS ^{14}C determinations.

Correspondence and requests for materials should be addressed to R.R. (e-mail: bert.roberts@latrobe.edu.au).